LETTERS
https://doi.org/10.1038/s41550-019-0820-1

nature astronomy

A Hubble constant measurement from superluminal motion of the jet in GW170817

K. Hotokezaka[1*], E. Nakar[2*], O. Gottlieb[2], S. Nissanke[3,4,5], K. Masuda[1], G. Hallinan[6], K. P. Mooley[6,7] and A. T. Deller[8,9]

The Hubble constant (H_0) measures the current expansion rate of the Universe, and plays a fundamental role in cosmology. Tremendous effort has been dedicated over the past decades to measure H_0 (refs. [1-10]). Gravitational wave (GW) sources accompanied by electromagnetic (EM) counterparts offer an independent standard siren measurement of H_0 (refs. [11-13]), as demonstrated following the discovery of the neutron star merger, GW170817 (refs. [14-16]). This measurement does not assume a cosmological model and is independent of a cosmic distance ladder. The first joint analysis of the GW signal from GW170817 and its EM localization led to a measurement of $H_0 = 74^{+16}_{-8}$ km s^{-1} Mpc^{-1} (median and symmetric 68% credible interval)[13]. In this analysis, the degeneracy in the GW signal between the source distance and the observing angle dominated the H_0 measurement uncertainty. Recently, tight constraints on the observing angle using high angular resolution imaging of the radio counterpart of GW170817 have been obtained[17]. Here, we report an improved measurement $H_0 = 70.3^{+5.3}_{-5.0}$ km s^{-1} Mpc^{-1} by using these new radio observations, combined with the previous GW and EM data. We estimate that 15 more GW170817-like events, having radio images and light curve data, as compared with 50–100 GW events without such data[18,19], will potentially resolve the tension between the Planck and Cepheid–supernova measurements.

Radio images have recently been obtained of a narrowly collimated jet associated with GW170817 by using very-long-baseline interferometry (VLBI), comprising the Very Long Baseline Array, the Karl G. Jansky Very Large Array and the Robert C. Byrd Green Bank Telescope, and a centroid motion of 2.7 ± 0.3 mas from day 75 to 230 has been reported[17], indicating the superluminal motion of the jet at an apparent velocity $\beta_{\rm app} = (4.1 \pm 0.5)\left(\frac{d}{41\ {\rm Mpc}}\right)$, where d is the source distance from Earth and the velocity is in units of the speed of light, c (1σ, including the uncertainty in the source distance). In addition, the slow rise[20] and fast decline[17,21] of the afterglow light curve provide us with evidence that a narrowly collimated jet dominates the emission after the light curve peak. These observed properties and the broadband single power-law spectrum[22] are well described by the synchrotron radiation arising from the forward shock of the jet. The superluminal motion depends strongly on the angle between us and the jet while the light curve depends also on the jet opening angle. Thus, we can obtain rather tight and robust constraints on the observing angle by combining the two (that is, the angle between our line-of-sight and the jet axis) independently of the GW analysis[17]. These constraints have some dependence on the exact jet modelling. To estimate this dependence and to see its effect in the measurement of H_0, we constrain the angle using several different and complementary methods: analytic modelling, full hydrodynamic numerical simulations and semi-analytic calculations of synthetic jet models.

The analytic modelling and numerical simulations are described in ref. [17]. The authors derive first rough analytic constraints on the observing angle, $\theta_{\rm obs}$, and then carry out a set of full hydrodynamical simulations of jets to find what geometries can fit the entire dataset. Their conclusion is that only models with $0.25 < \theta_{\rm obs}\left(\frac{d}{41\ {\rm Mpc}}\right) < 0.5$ rad $\left(15^\circ < \theta_{\rm obs}\left(\frac{d}{41\ {\rm Mpc}}\right) < 29^\circ\right)$ can fit the entire dataset (see Methods for the details of the hydro-jet modelling assisted by the analytic modelling). The viewing angles outside this range are inconsistent with the measured offset by at least 2σ.

To obtain the probability distribution of $\theta_{\rm obs}$ and d, and to estimate the effect of the jet modelling on the observational constraints on the observing angle, we ran Markov chain Monte Carlo (MCMC) simulations with two synthetic jet models: a power-law jet (PLJ) model and a Gaussian jet (GJ) model (see Methods). While the hydrodynamics of the jet is not fully taken into account in the synthetic models, unlike the numerical simulations, they allow us to scan the entire parameter space. Therefore, this analysis and the estimate based on the hydrodynamic simulations[17] are complementary. Figure 1 shows the posterior distribution for d and $\theta_{\rm obs}$ (see Methods). The observing angle is constrained to $0.29^{+0.03}_{-0.02}$ rad and $0.30^{+0.04}_{-0.04}$ rad (1σ) for the PLJ and GJ models, respectively. The constraint on the observing angle for a given model is tighter than the one obtained by the hydrodynamical simulations, most likely because the simulations explored various outflow structures while each synthetic model explores a single outflow shape. We stress here that the three different methods, the analytic modelling, hydrodynamical simulations and synthetic modelling, are consistent with each other within uncertainties, indicating the robustness of the observing angle estimate based on the superluminal motion and light curve. The most likely observing angles found with the synthetic models are smaller by ~0.05 rad than the median based on the hydrodynamic simulations. We consider this difference

[1]Department of Astrophysical Sciences, Princeton University, Princeton, NJ, USA. [2]The Raymond and Beverly Sackler School of Physics and Astronomy, Tel Aviv University, Tel Aviv, Israel. [3]GRAPPA, Anton Pannekoek Institute for Astronomy and Institute of High-Energy Physics, University of Amsterdam, Amsterdam, The Netherlands. [4]Nikhef, Amsterdam, The Netherlands. [5]Department of Astrophysics/IMAPP, Radboud University Nijmegen, Nijmegen, The Netherlands. [6]Caltech, Pasadena, CA, USA. [7]National Radio Astronomy Observatory, Socorro, NM, USA. [8]Centre for Astrophysics and Supercomputing, Swinburne University of Technology, Hawthorn, Victoria, Australia. [9]ARC Centre of Excellence for Gravitational Wave Discovery (OzGrav), Hawthorn, Victoria, Australia. *e-mail: kentah@astro.princeton.edu; udini@wise.tau.ac.il

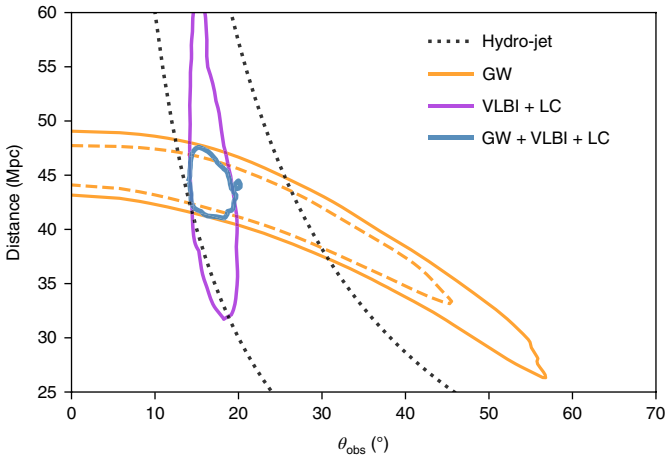

Fig. 1 | Distance and observing angle constraints to GW170817. Black dashed curves running from top to bottom depict the constraint of $0.25 < \theta_{obs}\left(\frac{d}{41\,\mathrm{Mpc}}\right) < 0.5$ rad estimated based on hydrodynamics simulations (assisted by the analytic modelling) and synthetic models[17]. The 95% regions obtained from the MCMC analysis of the afterglow light curve (LC) and centroid motion through VLBI are shown as solid purple (VLBI + LC). The blue contours (GW + VLBI + LC) are the same, but combined with the GW analysis for a PLJ model. Also shown as an orange dashed (solid) contour is the 68% (95%) contour of the posterior distribution of the GW-only analysis (high spin PhenomPNRT posterior samples)[23]. We note that the VLBI and LC data alone provide a distance estimate independent of all other means.

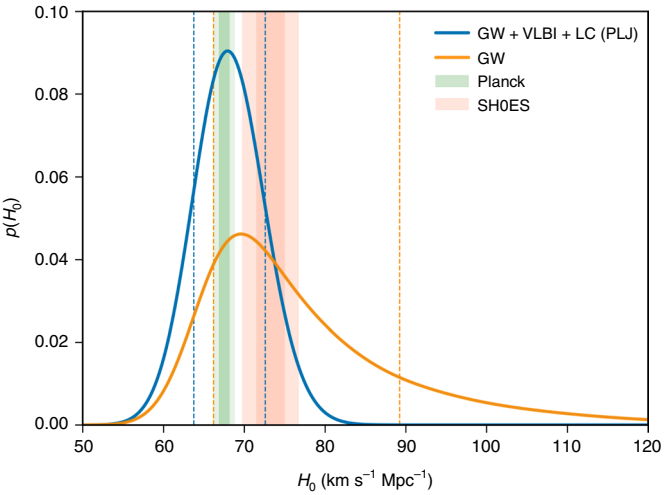

Fig. 2 | Posterior distributions for H_0. The results of the GW-only analysis (orange) and the combined GW–EM analysis with a PLJ model (blue) are shown. The vertical dashed lines show the symmetric 68% credible intervals for each model. The 1σ and 2σ regions determined by Planck CMB (TT,TE,EE+lowP+lensing model)[3] (green) and SH0ES Cepheid–supernova distance ladder surveys[4] (orange) are also depicted as vertical bands.

as a systematic uncertainty of our analysis (elaborated in the Methods), which is most likely attributed to the partial treatment of the hydrodynamic evolution in the synthetic models.

We now turn to the combined GW–EM analysis of the Hubble constant (H_0). Namely, we combine the two-dimensional marginalized GW likelihood distribution (high spin PhenomPNRT)[23] for d and θ_{obs} with that determined from the afterglow light curve and centroid motion (see Methods). The posterior distribution for H_0 is then computed from the combined likelihood for d and the information about the host galaxy NGC 4993 (see Methods)[13]. Figure 2 depicts the posterior distribution for H_0 for a PLJ model and that of the GW-only analysis[13,23]. The constraint is improved from the GW-only analysis, 74^{+16}_{-8} km s^{-1} Mpc^{-1}, to $68.1^{+4.5}_{-4.3}$ km s^{-1} Mpc^{-1} (median and symmetric 68% credible interval). Also depicted in Fig. 2 are the regions determined by the Planck cosmic microwave background (CMB)[3] and SH0ES Cepheid–supernova distance ladder surveys[4]. Figure 3 shows the posterior distributions for H_0 with the different jet models: hydrodynamics simulation jet $\left(0.25 < \theta_{obs}\left(\frac{d}{41\,\mathrm{Mpc}}\right) < 0.5\ \mathrm{rad}\right)$, and the PLJ and GJ models. The medians and 68% credible intervals are $70.3^{+5.3}_{-5.0}$, $68.1^{+4.5}_{-4.3}$ and $68.3^{+4.4}_{-4.3}$ km s^{-1} Mpc^{-1}, respectively, corresponding to a precision of 6–7% at the 1σ level. The sources of errors in our analysis are the GW data, the shape of the light curve, the centroid motion and the peculiar velocity of the host galaxy. While the constraint on θ_{obs} is slightly different between the three models, the systematic error in H_0 due to this difference is much smaller than 7%. This is because the uncertainty in H_0 of our analysis is dominated by both the GW data and the peculiar motion of NGC 4993 (contrary to the GW-only analysis, where the uncertainty in the observing angle is a major source of error). Finally, it is important to bear in mind that our result does not depend on the spin prior in the GW analysis[23] (see Methods).

Our analysis, which is based on this single event, improves the H_0 measurement to a precision of ~7% at the 1σ level, but it does not resolve the discrepancy between Planck and SH0ES yet. We expect that the precision of the measurement will improve by observing more merger events similar to GW170817, that is, mergers with detectable jet afterglows. In the coming years, several to tens of neutron star binary mergers (including neutron star–black hole binary systems) per year may be observable in GWs as the LIGO and Virgo detectors improve their sensitivity due to instrument upgrades, and as additional detectors join the GW network[24]. In addition, radio afterglow fluxes of merger events at farther distances are not necessarily fainter than GW170817 because of the wide variation in the circum-merger densities. For instance, the superluminal motion of a jet can be measured for events taking place out to ~100 Mpc if the density is about the typical value inferred from short gamma-ray burst observations[25] (and the other afterglow parameters are assumed to be the same as GW170817). We note, however, that a favourable observing angle is a likely prerequisite for detection. For events at greater d, while the error due to the radio observations increases, the error due to the peculiar motion decreases. Furthermore, inferring the binary inclination from GWs alone relies on the measurement of the GW polarization, which was particularly challenging in the case of GW170817 because of the low signal-to-noise ratio in the Virgo detector and the two LIGO detectors being nearly co-aligned[13,14]. For future GW radio jet events with similar signal-to-noise ratio, the H_0 uncertainty would thus remain comparable or better to that of this analysis because of the addition of GW detectors and of improved instrument sensitivity[18,19,26]. A rough estimate of the systematic uncertainty, based on the difference between hydrodynamics modelling and simple synthetic models, is of the order a few per cent, and hence the systematic uncertainty resulting from the jet modelling should also be reduced by a factor of 2–3 to achieve a measurement of H_0 with a high precision using more events.

Most current methods to estimate H_0 span from the local Universe to the CMB and include the use of Cepheid variables and red-giant stars[7], supernovae[4,5,27], circumnuclear megamasers[6], gravitational lenses[8,28], galaxies[2,9] and the CMB[1,3]. These methods either depend on a cosmic distance ladder relating geometric distances of Cepheid variables to standard candles, such as type Ia supernovae, or assume a certain cosmological model, such as the Λ cold dark matter (ΛCDM) model, where Λ is the cosmological constant[1–5,7–9]. The use of geometric distances to circumnuclear megamasers is a

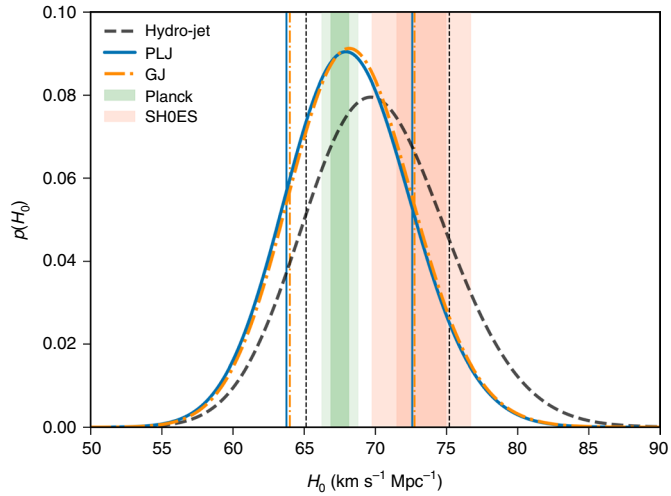

Fig. 3 | The Hubble constant with different jet models. Dashed black curve, hydrodynamics simulation assisted by the analytic modelling $\left(0.25 < \theta_{\rm obs}\left(\frac{d}{41\ {\rm Mpc}}\right) < 0.5\ {\rm rad}\right)$; solid blue curve, a PLJ model; dash-dotted orange curve, a GJ model. The vertical lines show the symmetric 68% credible intervals for each model. The 1σ and 2σ regions determined by Planck CMB (TT,TE,EE+lowP+lensing model)[3] (green) and SH0ES Cepheid–supernova distance ladder surveys[4] (orange) are also depicted as vertical bands. The synthetic modelling results in a slightly smaller value of H_0 than the hydrodynamic simulation as expected from the underestimate of the observing angle (Fig. 1). This difference is most likely attributed to the partial treatment of the jet evolution in the synthetic modelling.

notable exception, but is currently limited to 6% precision[6]. The current $\gtrsim 3\sigma$ discrepancy[4,29] between Planck CMB measurements and SH0ES data is of particular interest given the degree of precision in both measurements and the possible implication of the requirement of new physics beyond ΛCDM models if the discrepancy turns out to be true (rather than a result of systematic errors)[30]. Gaia data on galactic Cepheids, together with dedicated Hubble Space Telescope observations on the SH0ES data, will likely reduce systematic uncertainties sufficiently to improve the standard candle/distance ladder measurements of H_0 to ~1% precision at the 1σ level within the next few years[27], potentially raising this discrepancy above 5σ. In addition, the Zwicky Transient Facility and Large Synoptic Survey Telescope will find a large number of strongly lensed supernovae such as the supernova Refsdal[31] and iPTF16geu[32], which will lead to a H_0 measurement with a high precision[33]. A standard siren-based measurement of H_0, on a similar timescale, would be particularly useful, as it would independently provide a local measurement of H_0 that does not rely on a cosmic distance ladder, and which does not assume any cosmological model as a prior (although there are model assumptions in the interpretation of the VLBI data). We estimate that, after observing ~15 more GW170817-like events with VLBI data and light curves (comparable signal-to-noise ratio, favourable orientation), as compared with ~50–100 GW events without such data, the precision of the H_0 measurement would be ~1.8%[18,19,26]. (Of course, not all the future GW events will have a favourable orientation and strong EM signals. Note that, however, the fraction of the GW events with the observing angle <30° is expected to be ~40%[12].) Thus, joint GW–VLBI constraints on H_0 will potentially resolve the current tension between the Planck and standard candle/distance ladder data.

Methods

Observing angle constraint derived from the analytic modelling and hydrodynamic simulations. The analytic modelling and numerical simulations are described in ref. [17]. Given the importance of the new constraints on the observing angle on our results, we give here a brief summary of their results. The authors find that the model that best fits the observations is that of a successful jet[17]. We define $\theta_{\rm j}$ as the jet opening angle, $\theta_{\rm obs}$ as the observing angle and the difference between them as $\delta_\theta = \theta_{\rm obs} - \theta_{\rm j}$. The authors of ref. [17] show that the light curve and the small image size imply that the jet must be very narrow, that is, $\theta_{\rm j} \ll \delta_\theta$. This implies that the superluminal motion of the jet image can be approximated as that of a point source, where $\delta_\theta \approx 1/\Gamma$ (where Γ is the Lorentz factor of the jet) at the time of the observations (near the peak of the light curve). This implies $\delta_\theta \approx 1/\beta_{\rm app} \approx 0.25$ rad and $\theta_{\rm j} \ll 0.25$ rad, where a source distance of 41 Mpc is assumed. To verify this conclusion and to quantify the allowed region for δ_θ and $\theta_{\rm j} \ll 0.25$ rad, they then carried out a set of numerical simulations varying both the opening angle of the jet and the observing angle, allowing for a systematic check of which models can fit both the light curve and the images. They find that only models with $1/5 < \delta_\theta < 2/5$ rad and $\theta_{\rm j} < 0.1$ rad are consistent with observations within the $\sim 2\sigma$ level. They conclude that the combination of the VLBI measurements and the light curve data dictates $0.25 < \theta_{\rm obs} < 0.5$ rad ($15° < \theta_{\rm obs} < 29°$). This constraint is derived assuming that the distance to the source, d, is known (41 Mpc). However, in our analysis the distance is unknown and since the main constraint on the observing angle is derived from the the apparent velocity, $\beta_{\rm app} \propto d$, the observing angle is constrained to $0.25 < \theta_{\rm obs}\left(\frac{d}{41\ {\rm Mpc}}\right) < 0.5$ rad.

Observing angle constraint derived from the synthetic modelling. In the case of the afterglow of GW170817, the observed light curve rules out the simple top-hat jet model and supports structured jet models[20–22,34–44], of which the structure is likely composed of the jet core and surrounding cocoon[18,44–46]. We use two different structured jet models: a PLJ model and a GJ model, which can mimic the jet–cocoon structure obtained from numerical simulations[18,44–46]. The isotropic-equivalent energy and initial Lorentz factor vary with the polar angle for a PLJ model:

$$E_{\rm iso}(\theta) = \frac{E_{\rm iso,c}}{1 + (\theta/\theta_{\rm c})^{\alpha_E}} \quad (1)$$

$$\Gamma_{\rm j}(\theta) = 1 + \frac{\Gamma_{\rm j,c}}{1 + (\theta/\theta_{\rm c})^{\alpha_g}} \quad (2)$$

where $E_{\rm iso,c}$, $\theta_{\rm c}$, α_E and α_g are free parameters and we fix $\Gamma_{\rm j,c}$ to be 600. For a GJ model:

$$E_{\rm iso}(\theta) = E_{\rm iso,c}\exp\left[-\frac{1}{2}\left(\frac{\theta}{\theta_{\rm c}}\right)^2\right] \quad (3)$$

$$\Gamma_{\rm j}(\theta) = 1 + (\Gamma_{\rm j,c} - 1)\exp\left[-\frac{1}{2}\left(\frac{\theta}{\theta_{\rm c}}\right)^2\right] \quad (4)$$

where $E_{\rm iso,c}$, $\theta_{\rm c}$ are free parameters and we fix $\Gamma_{\rm j,c}$ to be 100.

For a given set of the model parameters and circum-merger density, n, we evolve the jet adiabatically and neglect the lateral expansion[41]. This assumption is valid until the jet slows down sufficiently. For the core of the jet, the lateral expansion occurs on a timescale much longer than what we have considered here, and indeed, we also find a lack of significant lateral expansion in the hydrodynamical simulations[17]. For the wing of the jet, however, the lateral expansion is important on the timescales considered here[17]. Therefore, our approximation here is expected to slightly underestimate the observing angle.

Given a jet evolution, we calculate the afterglow light curve and the motion of the flux centre by using the standard synchrotron afterglow model[47]. The code is described in ref. [48]. In the case of GW170817, the afterglow has a single power-law spectrum with a spectral index of 0.588 ± 0.005 from the radio to the X-ray bands[21,22,38], which is consistent with optically thin synchrotron emission in the slow cooling regime. Thus, here we consider only this regime. The synchrotron modelling involves three microphysics parameters (p, $\epsilon_{\rm e}$, $\epsilon_{\rm b}$), where $\epsilon_{\rm e}$ and $\epsilon_{\rm b}$ are the conversion efficiency from the internal energy to the energy of accelerated electrons and magnetic field, and p is the power-law index of the number distribution of accelerated electrons. Since the power-law index, p, is related to the observed spectrum as $F_\nu \propto \nu^{-(p-1)/2}$ (where F_ν is the flux density and ν is the frequency), we adopt $p = 2.16$. We also fix $\epsilon_{\rm e}$ to be 0.1.

Assuming the above models, we run MCMC simulations by using an open code emcee[49]. In this work, we are interested primarily in the viewing angle estimate, which is determined by the light curve shape and the motion of the flux centre. This allows us to reduce the number of free parameters, for example, parameters that do not affect the viewing angle estimate, $\epsilon_{\rm e}$ and $\Gamma_{\rm j,c}$, can be fixed as long as $\Gamma_{\rm j,c} \gg 4$. Here we use $E_{\rm iso,c}/n$, which determines the deceleration timescale of the jet, instead of using $E_{\rm iso,c}$ and n separately. Furthermore, instead of using $\epsilon_{\rm b}$, we introduce an auxiliary parameter, $e_{\rm b}$, which controls the overall amplitude of the light curve. Therefore, in total, we have seven parameters ($E_{\rm iso,c}/n$, $\theta_{\rm c}$, α_E, α_g, $e_{\rm b}$, $\theta_{\rm obs}$, d) for the PLJ model and five parameters ($E_{\rm iso,c}/n$, $\theta_{\rm c}$, $e_{\rm b}$, $\theta_{\rm obs}$, d) for the GJ

model. We adopt a log flat prior for $E_{\rm iso,c}/n$ and $e_{\rm b}$, and uniform prior for $\theta_{\rm c}$, α_E, $\alpha_{\rm g}$, an isotropic prior for $\theta_{\rm obs}$, and a volumetric prior for d. Because we find that the reduced χ^2 value for the light curve modelling is ~2–3, in addition to the model parameters we introduce a parameter e, which is added to the measurement uncertainty of each light curve data point. This leads to more conservative parameter estimates of the synthetic models.

Figure 1 (VLBI + LC) shows the resulting posterior for d and $\theta_{\rm obs}$ marginalized over the other model parameters. The corner plots for the model parameters are shown in Supplementary Figs. 1 and 2.

Combined GW–EM analysis of the Hubble constant. Next we performed the modelling of the light curve $x_{\rm LC}$ and centroid motion data $x_{\rm VLBI}$, taking into account the constraint from the GW data $x_{\rm GW}$. Because the GW and EM data are independent and only d and $\theta_{\rm obs}$ in the GW model affect the EM data, this can be done by replacing the prior on d and $\theta_{\rm obs}$ in the above MCMC analysis with the marginal posterior distribution from the GW analysis, $p(d, \theta_{\rm obs}|x_{\rm GW})$. Figure 1 (GW + VLBI + LC) shows the resulting posterior distribution $p(d, \theta_{\rm obs}|x_{\rm GW}, x_{\rm VLBI}, x_{\rm LC})$ marginalized over the other model parameters. The corresponding corner plots for the model parameters are shown in Supplementary Figs. 3 and 4. The posterior models for the afterglow flux at 3 GHz and centroid motion from day 75 to 230 measured with VLBI[17,20,34] are shown in Supplementary Fig. 5 with the data.

We combine $p(d, \theta_{\rm obs}|x_{\rm GW}, x_{\rm VLBI}, x_{\rm LC})$ from this joint modelling with the recessional velocity $v_{\rm r}$ to derive the Hubble constant H_0. To do so, one needs to take into account the unknown peculiar velocity of NGC 4993 as $v_{\rm r} = H_0 d + v_{\rm p}$. Here we follow the procedure used in ref. [14] to compute the marginalized posterior for H_0:

$$\begin{aligned} &p(H_0|x_{\rm GW}, x_{\rm VLBI}, x_{\rm LC}, v_{\rm r}, \langle v_{\rm p}\rangle) \\ &= \int {\rm d}d{\rm d}\cos\theta_{\rm obs}\, {\rm d}v_{\rm p}\, p(H_0, d, \cos\theta_{\rm obs}, v_{\rm p}|x_{\rm GW}, x_{\rm VLBI}, x_{\rm LC}, v_{\rm r}, \langle v_{\rm p}\rangle) \\ &\propto p(H_0)\int {\rm d}d\ {\rm d}v_{\rm p}\, p(v_{\rm r}|d, v_{\rm p}, H_0) p(\langle v_{\rm p}\rangle|v_{\rm p}) p(v_{\rm p}) p(d|x_{\rm GW}, x_{\rm VLBI}, x_{\rm LC}) \end{aligned} \quad (5)$$

We adopt the same information on $v_{\rm r}$ and $\langle v_{\rm p}\rangle$ as in ref. [14]:

$$p(v_{\rm r}|d, v_{\rm p}, H_0) = \frac{1}{\sqrt{2\pi\sigma_{v_{\rm r}}^2}}\exp\left[-\frac{1}{2}\left(\frac{v_{\rm r}-v_{\rm p}-H_0 d}{\sigma_{v_{\rm r}}}\right)^2\right] \quad (6)$$

$$p(\langle v_{\rm p}\rangle|v_{\rm p}) = \frac{1}{\sqrt{2\pi\sigma_{v_{\rm p}}^2}}\exp\left[-\frac{1}{2}\left(\frac{\langle v_{\rm p}\rangle-v_{\rm p}}{\sigma_{v_{\rm p}}}\right)^2\right] \quad (7)$$

where $v_{\rm r} = 3{,}327\,{\rm km\,s^{-1}}$, $\sigma_{v_{\rm r}} = 72\ {\rm km\ s^{-1}}$, $\langle v_{\rm p}\rangle = 310\,{\rm km\,s^{-1}}$ and $\sigma_{v_{\rm p}} = 150\ {\rm km\ s^{-1}}$.

The uncertainty in the peculiar velocity, $\sigma_{v_{\rm p}}$, is one of the largest error sources in the H_0 estimate of our GW and EM analysis. Note that, however, the contribution of this uncertainty to the error budget becomes smaller for future events occurring at distances farther away as $\propto 1/d$. On the contrary, the uncertainty in the GW distance and the superluminal motion goes as $\propto d$ (assuming a fixed afterglow flux). For instance, the error due to the peculiar velocity is smaller by a factor of two than the errors due to the GW distance and the EM viewing angle measurements for events similar to GW170817 at a distance of ~80 Mpc.

The posterior distribution for H_0 generally depends on the prior in the GW analysis[24], that is, the high or low spin prior. Supplementary Fig. 6 compares the H_0 posterior of the high spin prior with that of the low spin prior[24]. In the case of the GW-only analysis, the posterior distribution for H_0 depends on the prior as 78^{+20}_{-10} km s^{-1} Mpc^{-1} for the low spin prior and 74^{+15}_{-8} km s^{-1} Mpc^{-1} for the high spin prior (median and symmetric 68% credible interval). However, in the case of the combined analysis, the posterior distribution for H_0 results in practically the same H_0, $70.3^{+5.3}_{-5.0}$ km s^{-1} Mpc^{-1} (median and symmetric 68% credible interval). We also did the same analysis by using the GW posterior data of ref. [50]. These data result in slightly smaller values of H_0 compared with those in refs. [24,24]. Finally, our results are consistent with those obtained by using the surface brightness fluctuation technique applied to NGC 4993 (ref. [51]).

Data availability

MCMC samples are available from the corresponding author on request.

Code availability

The codes used for generating the synthetic light curves are currently being readied for public release. Markov chain Monte Carlo Ensemble sampler: emcee.

Received: 26 November 2018; Accepted: 16 May 2019;
Published online: 8 July 2019

References

1. Hinshaw, G. et al. Nine-year Wilkinson Microwave Anisotropy Probe (WMAP) observations: cosmological parameter results. *Astrophys. J. Suppl. Ser.* **208**, 19 (2013).
2. Aubourg, É. et al. Cosmological implications of baryon acoustic oscillation measurements. *Phys. Rev. D* **92**, 123516 (2015).
3. Planck Collaboration, Planck 2015 results. XIII. Cosmological parameters. *Astron. Astrophys.* **594**, A13 (2016).
4. Riess, A. G. et al. A 2.4% determination of the local value of the Hubble constant. *Astrophys. J.* **826**, 56 (2016).
5. Beaton, R. L. et al. The Carnegie–Chicago Hubble Program. I. An independent approach to the extragalactic distance scale using only population II distance indicators. *Astrophys. J.* **832**, 210 (2016).
6. Gao, F. et al. The Megamaser Cosmology Project. VIII. A geometric distance to NGC 5765b. *Astrophys. J.* **817**, 128 (2016).
7. Jang, I. S. & Lee, M. G. The Tip of the Red Giant Branch distances to Type Ia supernova host galaxies. V. NGC 3021, NGC 3370, and NGC 1309 and the value of the Hubble constant. Preprint at https://arxiv.org/abs/1702.01118 (2017).
8. Bonvin, V. et al. H0LiCOW – V. New COSMOGRAIL time delays of HE 0435–1223: H_0 to 3.8 per cent precision from strong lensing in a flat ΛCDM model. *Mon. Not. R. Astron. Soc.* **465**, 4914–4930 (2017).
9. Addison, G. E. et al. Elucidating ΛCDM: impact of baryon acoustic oscillation measurements on the Hubble constant discrepancy. *Astrophys. J.* **853**, 119 (2018).
10. DES Collaboration, Dark Energy Survey year 1 results: a precise H0 estimate from DES Y1, BAO, and D/H data. *Mon. Not. R. Astron. Soc.* **480**, 3879–3888 (2018).
11. Schutz, B. F. Determining the Hubble constant from gravitational wave observations. *Nature* **323**, 310–311 (1986).
12. Nissanke, S., Holz, D. E., Hughes, S. A., Dalal, N. & Sievers, J. L. Exploring short gamma-ray bursts as gravitational-wave standard sirens. *Astrophys. J.* **725**, 496–514 (2010).
13. Abbott, B. P. et al. A gravitational-wave standard siren measurement of the Hubble constant. *Nature* **551**, 85–88 (2017).
14. Abbott, B. P. et al. GW170817: observation of gravitational waves from a binary neutron star inspiral. *Phys. Rev. Lett.* **119**, 161101 (2017).
15. Abbott, B. P. et al. Multi-messenger observations of a binary neutron star merger. *Astrophys. J. Lett.* **848**, L12 (2017).
16. Guidorzi, C. et al. Improved constraints on H_0 from a combined analysis of gravitational-wave and electromagnetic emission from GW170817. *Astrophys. J. Lett.* **851**, L36 (2017).
17. Mooley, K. P. et al. Superluminal motion of a relativistic jet in the neutron star merger GW170817. *Nature* **561**, 355–359 (2018).
18. Chen, H.-Y., Fishbach, M. & Holz, D. E. Precision standard siren cosmology. *Nature* **562**, 545–547 (2018).
19. Feeney, S. M. et al. Prospects for resolving the Hubble constant tension with standard sirens. *Mon. Not. R. Astron. Soc.* **476**, 3861–3882 (2018).
20. Mooley, K. P. et al. A mildly relativistic wide-angle outflow in the neutron-star merger event GW170817. *Nature* **554**, 207–210 (2018).
21. Alexander, K. D. et al. A decline in the X-ray through radio emission from GW170817 continues to support an off-axis structured jet. *Astrophys. J. Lett.* **863**, L18 (2018).
22. Margutti, R. et al. The binary neutron star event LIGO/Virgo GW170817 160 days after merger: synchrotron emission across the electromagnetic spectrum. *Astrophys. J. Lett.* **856**, L18 (2018).
23. LIGO Scientific Collaboration and Virgo Collaboration Properties of the binary neutron star merger GW170817. *Phys. Rev. X* **9**, 011001 (2018).
24. Abbott, B. P. et al. Prospects for observing and localizing gravitational-wave transients with Advanced LIGO, Advanced Virgo and KAGRA. *Living Rev. Relativity* **21**, 3 (2018).
25. Fong, W., Berger, E., Margutti, R. & Zauderer, B. A. A decade of short-duration gamma-ray burst broadband afterglows: energetics, circumburst densities, and jet opening angles. *Astrophys. J.* **815**, 102 (2015).
26. Nissanke, S. et al. Determining the Hubble constant from gravitational wave observations of merging compact binaries. Preprint at https://arxiv.org/abs/1307.2638 (2013).
27. Riess, A. G. et al. Milky Way Cepheid standards for measuring cosmic distances and application to *Gaia* DR2: implications for the Hubble constant. *Astrophys. J.* **861**, 126 (2018).
28. Vega-Ferrero, J., Diego, J. M., Miranda, V. & Bernstein, G. M. The Hubble constant from SN Refsdal. *Astrophys. J. Lett.* **853**, L31 (2018).
29. Feeney, S. M., Mortlock, D. J. & Dalmasso, N. Clarifying the Hubble constant tension with a Bayesian hierarchical model of the local distance ladder. *Mon. Not. R. Astron. Soc.* **476**, 3861–3882 (2018).
30. Weinberg, D. H. et al. Observational probes of cosmic acceleration. *Phys. Rep.* **530**, 87–255 (2013).

31. Kelly, P. L. et al. Multiple images of a highly magnified supernova formed by an early-type cluster galaxy lens. *Science* **347**, 1123–1126 (2015).
32. Goobar, A. et al. iPTF16geu: a multiply imaged, gravitationally lensed type Ia supernova. *Science* **356**, 291–295 (2017).
33. Goldstein, D. A., Nugent, P. E., Kasen, D. N. & Collett, T. E. Precise time delays from strongly gravitationally lensed type Ia supernovae with chromatically microlensed images. *Astrophys. J.* **855**, 22 (2018).
34. Hallinan, G. et al. A radio counterpart to a neutron star merger. *Science* **358**, 1579–1583 (2017).
35. Ruan, J. J., Nynka, M., Haggard, D., Kalogera, V. & Evans, P. Brightening X-ray emission from GW170817/GRB 170817A: further evidence for an outflow. *Astrophys. J. Lett.* **853**, L4 (2018).
36. D'Avanzo, P. et al. The evolution of the X-ray afterglow emission of GW 170817/GRB 170817A in XMM-Newton observations. *Astron. Astrophys.* **613**, L1 (2018).
37. Dobie, D. et al. A turnover in the radio light curve of GW170817. *Astrophys. J. Lett.* **858**, L15 (2018).
38. Troja, E. et al. The outflow structure of GW170817 from late-time broad-band observations. *Mon. Not. R. Astron. Soc.* **478**, L18–L23 (2018).
39. Lamb, G. P. & Kobayashi, S. GRB 170817A as a jet counterpart to gravitational wave trigger GW 170817. *Mon. Not. R. Astron. Soc.* **478**, 733–740 (2018).
40. Lyman, J. D. et al. The optical afterglow of the short gamma-ray burst associated with GW170817. *Nat. Astron.* **2**, 751–754 (2018).
41. Gill, R. & Granot, J. Afterglow imaging and polarization of misaligned structured GRB jets and cocoons: breaking the degeneracy in GRB 170817A. *Mon. Not. R. Astron. Soc.* **478**, 4128–4141 (2018).
42. Resmi, L. et al. Low frequency view of GW 170817/GRB 170817A with the Giant Meterwave Radio Telescope. *Astrophys. J. Lett.* **867**, 57 (2018).
43. Nakar, E. & Piran, T. Implications of the radio and X-ray emission that followed GW170817. *Mon. Not. R. Astron. Soc.* **478**, 407–415 (2018).
44. Xie, X., Zrake, J. & MacFadyen, A. Numerical simulations of the jet dynamics and synchrotron radiation of binary neutron star merger event GW170817/GRB170817A. *Astrophys. J.* **863**, 58 (2018).
45. Gottlieb, O., Nakar, E. & Piran, T. The cocoon emission—an electromagnetic counterpart to gravitational waves from neutron star mergers. *Mon. Not. R. Astron. Soc.* **473**, 576–584 (2018).
46. Lazzati, D. et al. Late time afterglow observations reveal a collimated relativistic jet in the ejecta of the binary neutron star merger GW170817. *Phys. Rev. Lett.* **120**, 241103 (2018).
47. Sari, R., Piran, T. & Narayan, R. Spectra and light curves of gamma-ray burst afterglows. *Astrophys. J. Lett.* **497**, L17–L20 (1998).
48. Hotokezaka, K. & Piran, T. Mass ejection from neutron star mergers: different components and expected radio signals. *Mon. Not. R. Astron. Soc.* **450**, 1430–1440 (2015).
49. Foreman-Mackey, D., Hogg, D. W., Lang, D. & Goodman, J. emcee: the MCMC hammer. *Publ. Astron. Soc. Pac.* **125**, 306–312 (2013).
50. Finstad, D. et al. Measuring the viewing angle of GW170817 with electromagnetic and gravitational waves. *Astrophys. J. Lett.* **860**, L2 (2018).
51. Cantiello, M. et al. A precise distance to the host galaxy of the binary neutron star merger GW170817 using surface brightness fluctuations. *Astrophys. J. Lett.* **854**, L31 (2018).

Acknowledgements

We are grateful to D. Brown, C. Hirata, V. Scowcroft, P. Shawhan, D. Spergel and H. Peiris for useful discussions. We thank the LIGO Scientific and Virgo Collaborations for public access to their data products. K.H. is supported by the Lyman Spitzer Jr. Fellowship at the Department of Astrophysical Sciences, Princeton University. E.N. and O.G. are supported by the I-Core center of excellence of the CHE-ISF. S.N. is grateful for support from NWO VIDI and TOP Grants of the Innovational Research Incentives Scheme (Vernieuwingsimpuls) financed by the Netherlands Organization for Scientific Research (NWO). The work of K.M. is supported by NASA through the Sagan Fellowship Program executed by the NASA Exoplanet Science Institute, under contract with the California Institute of Technology (Caltech)/Jet Propulsion Laboratory (JPL). G.H. acknowledges the support of NSF award AST-1654815. A.T.D. is the recipient of an Australian Research Council Future Fellowship (FT150100415).

Author contributions

K.H. carried out MCMC simulations with the synthetic models. E.N. and O.G. derived an analytic model and carried out hydrodynamic simulations to derive constraints on the observing angle. K.H. and K.M. analysed the posterior samples and calculated H_0. G.H., K.P.M. and A.T.D. provided the input observational data. K.H., E.N., S.N. and G.H. wrote the paper. All co-authors discussed the results and provided comments on the manuscript.

Competing interests

The authors declare no competing interests.

Additional information

Supplementary information is available for this paper at https://doi.org/10.1038/s41550-019-0820-1.

Reprints and permissions information is available at www.nature.com/reprints.

Correspondence and requests for materials should be addressed to K.H. or E.N.

Peer review information: *Nature Astronomy* thanks Peter Nugent and the other, anonymous, reviewer(s) for their contribution to the peer review of this work.

Publisher's note: Springer Nature remains neutral with regard to jurisdictional claims in published maps and institutional affiliations.